Architecture and genomic arrangement of the MurE–MurF bacterial cell wall biosynthesis complex

Karina Shirakawa, Fernanda Angélica Sala, Mayara Miyachiro, Viviana Job, Daniel Maragno Trindade, Andréa Dessen

PNAS RESEARCH ARTICLE | BIOCHEMISTRY

Architecture and genomic arrangement of the MurE–MurF bacterial cell wall biosynthesis complex

Karina T. Shirakawa[a,b], Fernanda Angélica Sala[a], Mayara M. Miyachiro[c], Viviana Job[c], Daniel Maragno Trindade[a,1], and Andréa Dessen[a,c,1]

Edited by Christoph Mayer, Eberhard Karls Universitat Tubingen Fachbereich Biologie, Tübingen, Germany; received November 15, 2022; accepted April 5, 2023 by Editorial Board Member Joseph J. Kieber

Peptidoglycan (PG) is a central component of the bacterial cell wall, and the disruption of its biosynthetic pathway has been a successful antibacterial strategy for decades. PG biosynthesis is initiated in the cytoplasm through sequential reactions catalyzed by Mur enzymes that have been suggested to associate into a multimembered complex. This idea is supported by the observation that in many eubacteria, *mur* genes are present in a single operon within the well conserved *dcw* cluster, and in some cases, pairs of *mur* genes are fused to encode a single, chimeric polypeptide. We performed a vast genomic analysis using >140 bacterial genomes and mapped Mur chimeras in numerous phyla, with Proteobacteria carrying the highest number. MurE–MurF, the most prevalent chimera, exists in forms that are either directly associated or separated by a linker. The crystal structure of the MurE–MurF chimera from *Bordetella pertussis* reveals a head-to-tail, elongated architecture supported by an interconnecting hydrophobic patch that stabilizes the positions of the two proteins. Fluorescence polarization assays reveal that MurE–MurF interacts with other Mur ligases via its central domains with K_Ds in the high nanomolar range, backing the existence of a Mur complex in the cytoplasm. These data support the idea of stronger evolutionary constraints on gene order when encoded proteins are intended for association, establish a link between Mur ligase interaction, complex assembly and genome evolution, and shed light on regulatory mechanisms of protein expression and stability in pathways of critical importance for bacterial survival.

peptidoglycan | Mur ligases | chimeric proteins | *Bordetella* spp

Significance

Mur ligases are essential for bacterial cell wall biosynthesis. Mur enzymes have been hypothesized to form a complex, an idea supported by the observation that the order of *mur* genes is often conserved, and some are fused to generate chimeric proteins. Here we present an analysis of the distribution of natural Mur chimeras, as well as the first structure of a chimeric MurE–MurF, that displays a unique, tightly connected architecture. MurE–MurF interacts in a transient and domain-dependent manner with other Mur ligases, supporting the idea that gene order conservation is intricately related to Mur enzyme assembly in the cytoplasm. Our data shed light on mechanisms of protein complex formation in a cellular pathway of key importance for bacterial survival.

Antibiotic resistance is a major threat not only to global health but also to food security and economic development. One of the most successful antibiotic targets is the bacterial cell wall biosynthesis machinery. Its key component, the peptidoglycan (PG), is a three-dimensional cross-linked mesh of polymerized sugars and short peptides whose stability and preservation are essential for bacterial shape and tolerance to modifications in osmotic conditions (1, 2). PG biosynthesis is targeted by β-lactam antibiotics through the inhibition of Penicillin-binding proteins (PBPs), but numerous pathogenic bacteria can now circumvent β-lactam action by manipulating PBP sequences and structures, expression levels, and by secreting β-lactamases (3–5). It is thus essential to explore alternative targets and protein complexes within the PG biosynthesis pathway by characterizing other enzymes involved in the process.

PG biosynthesis involves 11 to 12 steps that take place in three different bacterial cell compartments (cytoplasm, membrane, and periplasm). In the cytoplasm, enzymes encoded by *mur* (murein) genes play key roles in the generation of Lipid II, the major PG building block (1, 6). Upon the formation of the main sugar backbone, UDP–MurNAc (or UM), through the action of MurA and MurB, ATP-dependent enzymes collectively called Mur ligases (MurC, D, E, and F) catalyze the stepwise ligation of amino acids onto this soluble precursor (7–9) (Fig. 1*A*). MurC adds L-alanine to form UDP-*N*-acetylmuramoyl-L-alanine (UMA), and this is followed by the addition of D-glutamate by MurD. The subsequent MurE-catalyzed reaction associates either *meso*-diaminopimelate (A2pm or DAP) or L-lysine to the growing chain, depending on the bacterial species. MurF catalyzes the last step towards the formation of the UM-pentapeptide by adding a D-alanyl-D-alanine dipeptide to the UM-tripeptide. This precursor is subsequently associated to undecaprenol-phosphate, a 55-carbon, membrane-bound lipid carrier molecule at the inner leaflet of the membrane by MraY, generating Lipid I. This molecule is then transformed into Lipid II through association of a GlcNAc group by MurG (8–10). The species catalyzed in this fashion is subsequently flipped toward the periplasmic space upon which it will be acted upon by PBPs, Lpo regulators, and SEDS (shape, elongation, division, and sporulation) family proteins to generate the polymerized and cross-linked form of PG (11–14). PG biosynthesis is further regulated by two dynamic complexes that harbor

Author contributions: K.T.S., D.M.T., and A.D. designed research; K.T.S., F.A.S., M.M.M., V.J., and D.M.T. performed research; K.T.S., F.A.S., D.M.T., and A.D. analyzed data; and K.T.S. and A.D. wrote the paper.

The authors declare no competing interest.

This article is a PNAS Direct Submission. C.M. is a guest editor invited by the Editorial Board.

[1]To whom correspondence may be addressed. Email: daniel.trindade@lnbio.cnpem.br or andrea.dessen@ibs.fr.

This article contains supporting information online at https://www.pnas.org/lookup/suppl/doi:10.1073/pnas.2219540120/-/DCSupplemental.

Published May 15, 2023.

both PBPs, SEDS, and other partner proteins, namely the divisome, involved in cell division, and the elongasome or Rod complex, that plays a key role in cell wall elongation in nonspherical bacteria (5, 11, 13, 15–17).

Mur ligases catalyze the key cytoplasmic steps of Lipid II biosynthesis in a stepwise manner. They are encoded by genes located within the *dcw* (*division and cell wall*) cluster, whose order and composition are generally well conserved in all eubacteria studied to date (24–27) (Fig. 1*B*). The longest version of the *dcw* cluster involves more than 15 genes and includes those that code for proteins responsible for the cytoplasmic PG biosynthesis steps (DdlB, MurA, MurB, MurC, MurD, MurE, MurF, MurG, and MraY), cell division (FtsA, FtsI, FtsL, FtsQ, FtsW, and FtsZ), and even proteins that play roles in DNA recognition or RNA methylation. Notably, a correlation between bacterial cell shape and the order of genes within the *dcw* cluster has been observed. Rod-shaped bacteria display a compact, highly conserved cluster, while species with other shapes present genetic rearrangements

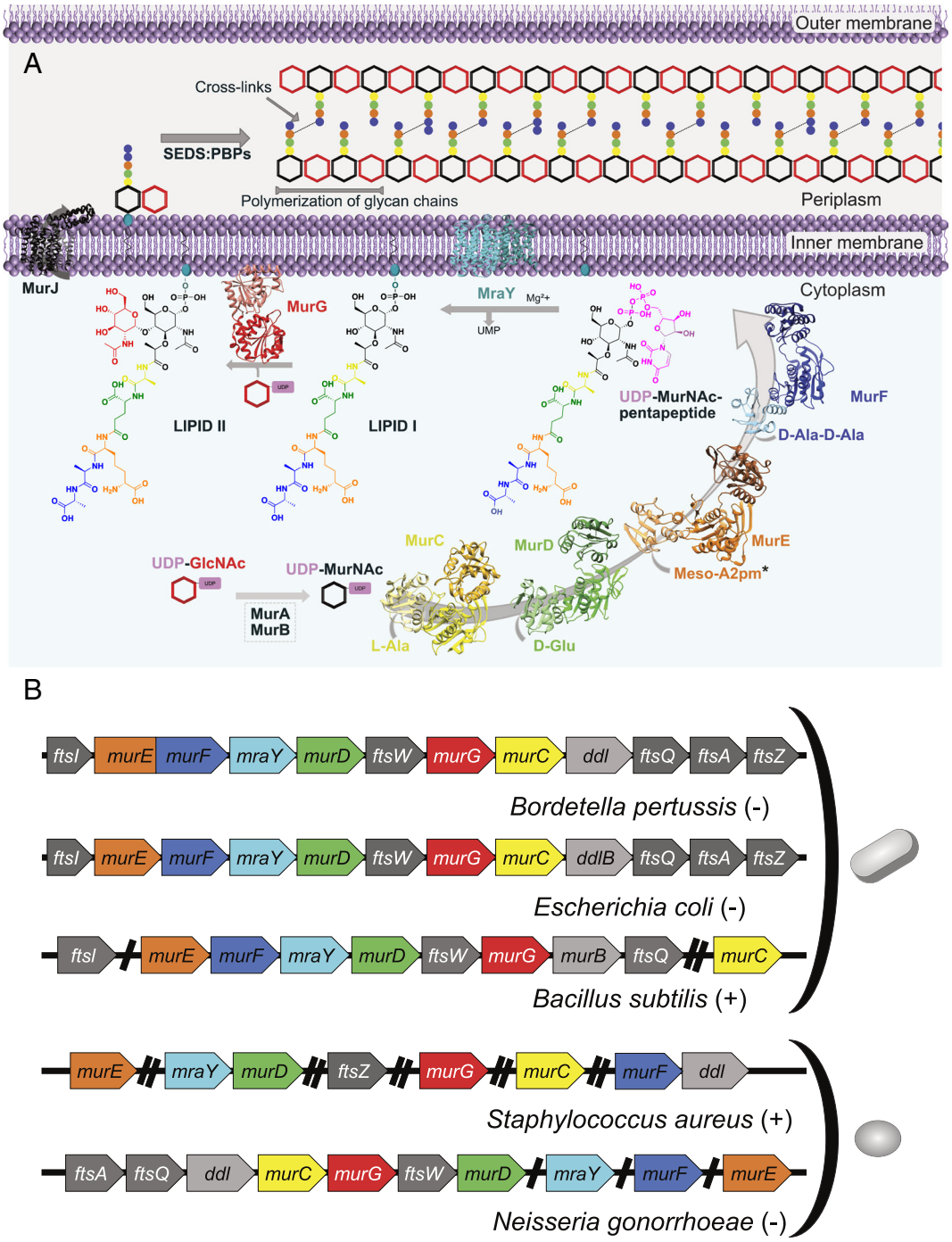

Fig. 1. Schematics of the PG biosynthetic process in gram-negatives and arrangement of the *dcw* genomic cluster. (*A*) Steps accomplished in the cytoplasm/membrane include reactions catalyzed by MurC [PDB: 2F00; (18)], MurD [PDB: 1E0D; (19)], MurE (PDB: 7B53), MurF [PDB: 1GG4; (20)], MraY [PDB: 4J72; (21)] and MurG [PDB: 1F0K; (22)]. Colors indicate the residue added by the corresponding protein: MurC in yellow (L-Ala), MurD in green (D-Glu), MurE in orange (meso-A2pm), and MurF in blue (D-Ala-D-Ala), and MurJ in black (PDB: 6CC4). * indicates that L-Lys is generally added instead of meso-A2pm in gram-positives. Peptide cross-linking forms reflect those indicated for *B. pertussis* in ref. 23. (*B*) Region within the *dcw* cluster that involves Mur ligase-expressing genes. The slanted bars indicate intervening genes; double slanted bars indicate the location of multiple genes. Note that rod-like, gram-negative bacteria present a conserved gene order, which is not the case for gram-positive and/or nonrod-like species. Genetic information was obtained from NCBI reference genomes.

that lead to a loss of gene order conservation. In some species and during specific growth phases, several genes in the cluster are co-transcribed as long polycistronic RNAs, originating from promoters located upstream from *murE* (26, 28) (Fig. 1*B*).

Several of the proteins encoded by genes within the *dcw* cluster have been shown to co-localize in bacteria, interact directly, or both. In *Caulobacter crescentus*, MurC, MurE, MurF, and MraY all localize in a fashion that is similar to that of MurG, which was also shown to play a role in the recognition of Mur ligases from *Thermotoga maritima* and *Bordetella pertussis* (29–31). In addition, Mur ligases C-F from *Streptococcus pneumoniae* have been shown to interact, with enzymes that catalyze earlier steps presenting higher affinity for each other than those in the later stages of Lipid I biosynthesis (32). Coupled to the suggested relationship between gene organization in prokaryotic operons and clusters and the formation of protein complexes (33), these observations have reinforced the hypothesis that Mur ligases could associate as a complex within the bacterial cytoplasm in order to more effectively shuttle PG-building blocks to the membrane (8, 29, 31, 32, 34, 35).

In order to investigate the Mur ligase complex formation hypothesis from genomics and structural viewpoints, we first screened hundreds of bacterial genomes in the search of strains harboring fused *mur* genes, encoding natural Mur chimeras; we reasoned that these candidates could display the most stable conformation between the proteins and would increase our chances of working with a more stable complex. By performing a vast search for fused *mur* genes in >140 genomes, we identified that gene chimeras are widespread in phyla ranging from Proteobacteria to Chlamydiae; particularly, MurE and MurF are encoded as a single polypeptide in numerous species of proteobacteria such as *B. pertussis*. We solved the crystal structure of MurE–MurF from *B. pertussis* and found that it displays an elongated fold with neighboring active sites. The MurE–MurF interaction region is highly hydrophobic and is composed of residues that juxtapose the two Mur ligases, hindering any possibility of rotation and further distancing of the active sites. Fluorescence polarization assays (FPAs) indicate that the MurE–MurF chimera interacts with both MurC and MurD with K_Ds in the high nanomolar range, with the central domains being mostly responsible for partner recognition. This points to the possible formation of a Mur complex composed of multiple distinct Murs. These results indicate how there could be catalytic and regulatory advantages for the bacterial cell in having two murein biosynthesis reactions catalyzed by fused proteins, and underline the importance of a multi-Mur ligase complex for optimal PG biosynthesis.

Results

Distribution of the Mur Ligase Chimeras. In order to understand the extent of the presence the chimeras throughout different bacterial phyla, we selected a representative sequence from each bacterial species that harbored annotated chimeras, generated sequence similarity networks (SSN) using EFI-EST (36) and analyzed the resulting networks using Cytoscape (37). In these analyses, we observed that different Mur chimera types are concentrated in specific phyla (Fig. 2): MurE–MurF are highly present in Proteobacteria; MurG–MurC in Actinobacteria; MurC–MurB in Verrucomicrobia; MurC–Ddl in Chlamydiae and Firmicutes; and MurD–FtsW in Proteobacteria and Actinobacteria. Further analyses of the protein sequences in the Uniprot database revealed that out of the five major types of Mur chimeras, MurE–MurF is the most abundant one, representing 64% of all chimeras, followed by MurC–Ddl (11%), MurC–MurB (11%), MurG–MurC (9%), and MurD–FtsW (3%) (Fig. 2 and *SI Appendix*, Fig. S1).

Most (96.4%) of all MurE–MurF chimeras exist in proteobacteria, and are well represented in β-proteobacteria (65.7%; Fig. 2). Within the nonpathogenic strains that carry MurE–MurF, a number of them are associated with polluted or contaminated sites, such as those identified from sewage [*Candidimonas* spp (38)], deep-sea oil-contaminated sites [*Pusillimonas* spp (39)] or leachate treatment sludge [*Castellaniella* spp (40)]. MurE–MurF could also be identified in genomes of pathogenic bacteria linked to cystic fibrosis, such as *Achromobacter* and *Alcaligenes* spp (41, 42) and is widespread in *Bordetella* spp, having been identified in 12 of the 16 different species characterized to date [the four remaining species are yet to be fully sequenced (43)]. It is notably present in the genomes of *Bordetella bronchiseptica*, *B. parapertussis*, and *B. pertussis*, all of which are adapted to colonize the mammalian respiratory tract. *B. pertussis* is the causative agent of whooping cough in humans, a disease transmitted by droplets that is common and dangerous, particularly in unvaccinated children (44). It is of interest that δ-proteobacteria, that include many strains of sulfate-reducing bacteria found in marine sediments and in mangrove ecosystems, and α-proteobacteria, that include methanotrophs, methylotrophs, and nitrogen-fixing species (45), also display MurE–MurF chimeras.

Chimeric proteins formed by MurE and MurF can display two different architectures: i) MurE and MurF joined by a long linker region that can reach up to hundreds of amino acids (Fig. 3), as in the case of *Stappia indica*, that carries a linker of ~300 residues, and ii) MurE and MurF associated head-to-tail with no linker. Structure prediction algorithms could not model any recognizable fold or domains within these linker sequences, frequently predicting them to be disordered. Regarding the linker-less, head-to-tail association between MurE and MurF, it is predicted to be vastly present in β-proteobacteria, and is consistently present in MurE–MurF chimeras of *Bordetella* and *Achromobacter* species (Fig. 3), which are close in phylogeny.

A Hydrophobic Patch Locks MurE and MurF in a Fixed Conformation. The crystal structures of isolated Mur ligases indicate that they display similar 3D structures with an N-terminal domain that binds the UM-peptide precursors, a central ATP-recognizing domain, and a C-terminal region that binds the amino acid(s) to be added onto the precursor (29, 46–48). A low-resolution, small-angle scattering model of MurE–MurF from *B. pertussis* had shown that the protein was elongated and flexible (30), but no high-resolution data were available. In order to obtain a stable sample that would generate well-diffracting crystals, the full-length, 6-domain form of MurE–MurF from *B. pertussis* (henceforth called MurE–$MurF_{FL}$, Fig. 4*A*) was submitted to limited proteolysis, and the resulting smaller, stable form was confirmed by mass spectrometry to lack the last 142 residues of MurE–$MurF_{FL}$ that correspond to the C-terminal domain of MurF. This sample, henceforth referred to as MurE–$MurF_{\Delta 6}$, was employed for further crystallization trials. Diffracting crystals were only obtained through two cycles of microseeding and manual reproduction (details in *Materials and Methods*). Synchrotron data were collected to 2.6 Å resolution and crystals were in space group I222, with one MurE–$MurF_{\Delta 6}$ molecule per asymmetric unit. The structure was solved by molecular replacement using a model of *B. pertussis* MurE–MurF generated by AlphaFold2 (49) split into three fragments, through a three-component search in Phaser (50). Iterative manual building and model improvement led to the structure whose statistics for data collection and refinement are presented in *SI Appendix*, Table S1.

The MurE–$MurF_{\Delta 6}$ chimera folds into an elongated structure (Fig. 4*B*) where all five visible domains are in an extended

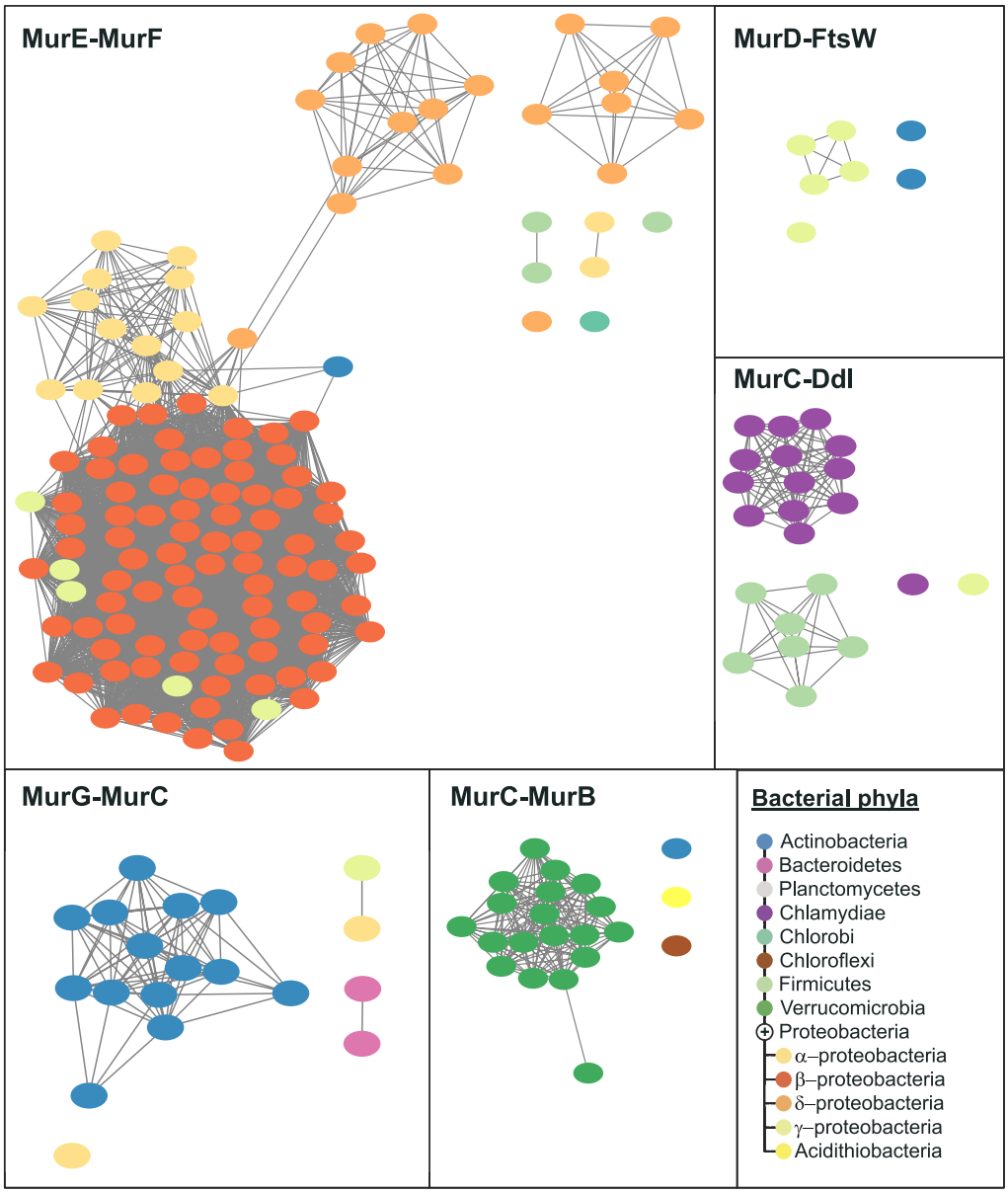

Fig. 2. Distribution of Mur chimeras in different bacterial phyla. Protein sequences were obtained from UniProt, and only representative sequences from identified species were used for figure generation. Sequence similarity networks were generated with EFI-EST (efi.igb.illinois.edu/efi-est/) and the resulting networks were analyzed with Cytoscape (37). The MurE–MurF chimera is the variant with the highest representation, and is notably present in α, β, and γ-proteobacteria.

conformation. Mur ligases have been shown to often modify their conformation depending on ligand binding, with apo forms being more "open," and ligand-bound forms displaying domain closure. Despite the fact that our MurE–MurF structure is in apo form, an overlay with ligand-bound structures of individual MurE and MurF variants from *S. aureus* and *P. aeruginosa* (47), crystallized in the presence of substrate and cofactors, allowed the localization of the active sites, that catalyze sequential reactions, practically on the same face of MurE–MurF (Fig. 4*C*). In the structure of the chimera, the two binding sites are approximately 50 Å apart from each other (measured from the central region of each cleft). This could facilitate transfer of the product of the MurE reaction directly towards MurF, thus preventing the growing building block, upon leaving the MurE active site, from being exchanged into the cytoplasm prior to being recognized by MurF. Notably, superposition of MurE–MurF with the open, intermediate, and closed forms of MurE or MurF (*SI Appendix*, Figs. S3 and S4) confirmed that the N terminus of MurE in the *B. pertussis* chimera is in an "open" conformation, that is often associated to structures of Mur ligases in the absence of ligand (51).

The interface between MurE and MurF consists of a mostly helical region that covers a hydrophobic patch, forming a tight nonpolar pocket (Fig. 5). This arrangement generates a seemingly rigid organization where the orientation between the two proteins could be stabilized, potentially to favor ligand transfer. A B-factor distribution analysis of the structure indicates the relative stability of the region surrounding the hydrophobic pocket (*SI Appendix*, Figs. S5 and S6). It is of note that in structures of isolated MurF variants from various bacteria, a hydrophobic patch at the N terminus of the molecule (yellow in Fig. 6) is covered by a small loop region, often harboring a single short helix, the "cap" (red in Fig. 6 and *SI Appendix*, Fig. S7). Both the hydrophobic region and the N-terminal cap are highly conserved in MurF variants (*SI Appendix*, Figs. S2, S7, and S8). Importantly, analyses of MurE–MurF chimera sequences from ~129 proteobacterial species indicate that residues that form the cap and hydrophobic regions are highly conserved (*SI Appendix*, Fig. S9).

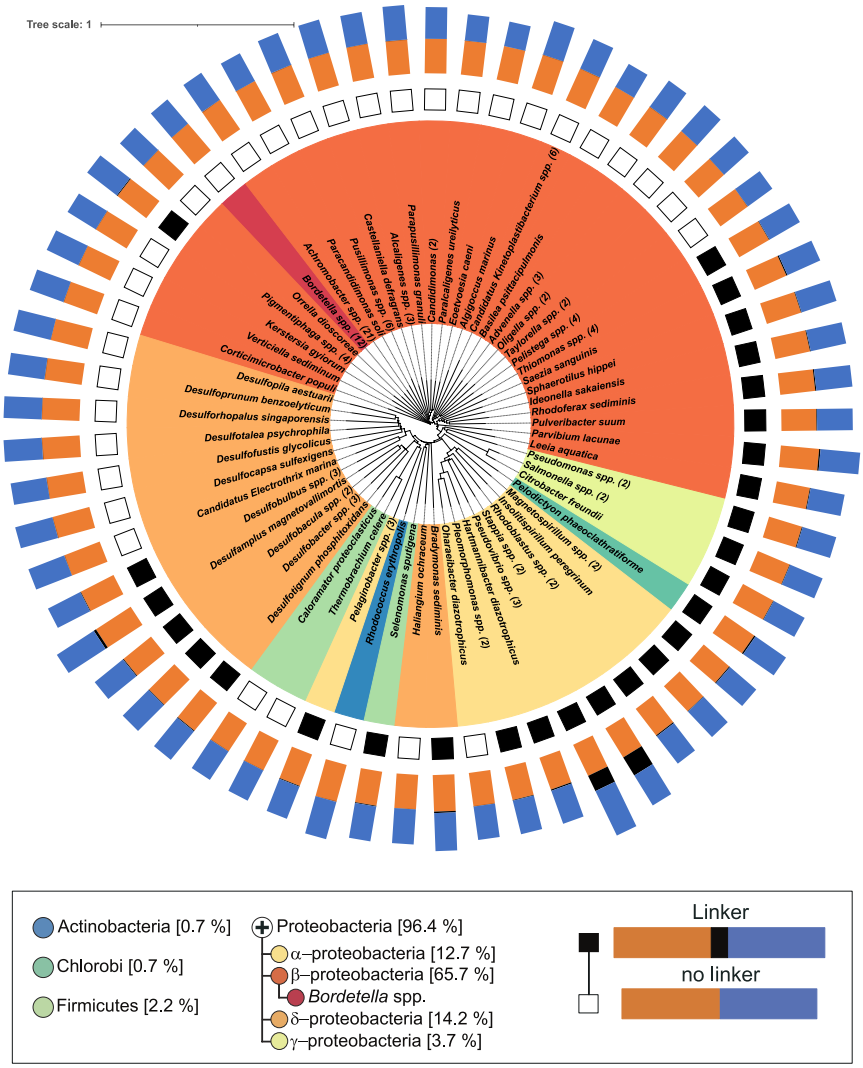

Fig. 3. Phylogenetic analysis and distribution of MurE–MurF chimeras in bacteria. MurE–MurF sequences are separated by phylum, with proteobacteria subclassified into α, β, δ and γ-proteobacteria. Chimeras were further classified according to the length of the linker (indicated as a black box) between the C-terminal domain of MurE and N-terminal domain of MurF. MurE is indicated in orange and MurF in blue. The bar chart around the phylogenetic tree indicates the length of the MurE–MurF sequence as well as of the linker. *Bordetella* spp are highlighted in red. The number of species employed in each analysis is highlighted in parentheses. Most of the species predicted to carry linker-less MurE–MurF chimeras are from β- and δ-proteobacteria. α and γ-proteobacteria are predicted to have MurE–MurF chimeras with varying sizes of linker, with *Stappia* spp and *Pseudovibrio* spp displaying 200 to 300 residue-long linkers.

In the case of the MurE–MurF chimera, MurF itself has no cap region; hence, the helical region that covers its hydrophobic patch is provided by the C terminus of MurE (Fig. 6, *Top*). This points to the importance of the N-terminal, hydrophobic region of MurF in fostering interactions with MurE in the cytoplasm of bacteria that do not express chimeras. In order for the two proteins to interact, we propose that the cap region of MurF could open in order to accommodate the C terminus of MurE in proximity to its hydrophobic N-terminal patch, as suggested by the structure of the chimera.

The MurE–MurF Chimera Recognizes Other Mur Ligases from *B. pertussis*. Mur ligases from organisms such as *T. maritima* and *S. pneumoniae* are able to interact with different Murs, observations that have prompted the suggestion of the existence of a Mur complex within the bacterial cytoplasm (29–32, 35). We thus set out to test the capacity of the MurE–MurF chimera to associate with other Mur ligases from *B. pertussis*, and to identify the major domains of the chimera involved in the interactions. We performed FPA using FITC-labeled MurC and MurD (Fig. 7), and these samples were tested against MurE–MurF constructs carrying different domains.

MurE–MurF$_{FL}$ associated with both MurC and MurD with K_D values of approximately 0.80 μM, which is compatible with the hypothesis of a transient Mur ligase complex within the bacterial cytoplasm. In order to map the domains of MurE–MurF that are relevant for the interaction with other Murs, we included MurE–MurF$_{\Delta 6}$ (5 domains) and MurE–MurF$_{\Delta 3456}$ (2 domains) in FPA experiments. Constructs of intermediary length that involved modifications in the vicinity of domains 3 and 4, that involve the hydrophobic patch and the cap, were not soluble or were unstable.

MurE–MurF$_{\Delta 6}$ bound to MurC and MurD with a similar affinity as MurE–MurF$_{FL}$ (approx. 0.7 μM). However, we could not measure a K_D for an interaction between MurE–MurF$_{\Delta 3456}$ with either MurC or MurD (Fig. 7 *B* and *C*). These results indicate that the interactions between MurE–MurF and the two other Mur ligases involve its three central domains (the C terminus of MurE and the two first domains of MurF, Fig. 4*A*), with the MurE–MurF interaction region thus playing an important role in complex stability. It is also of note that MurC and MurD can neither self-associate nor bind to one another with any measurable K_D, independently of the choice of labeled and titrated protein (*SI Appendix*, Fig. S10), indicating that preference is given for the

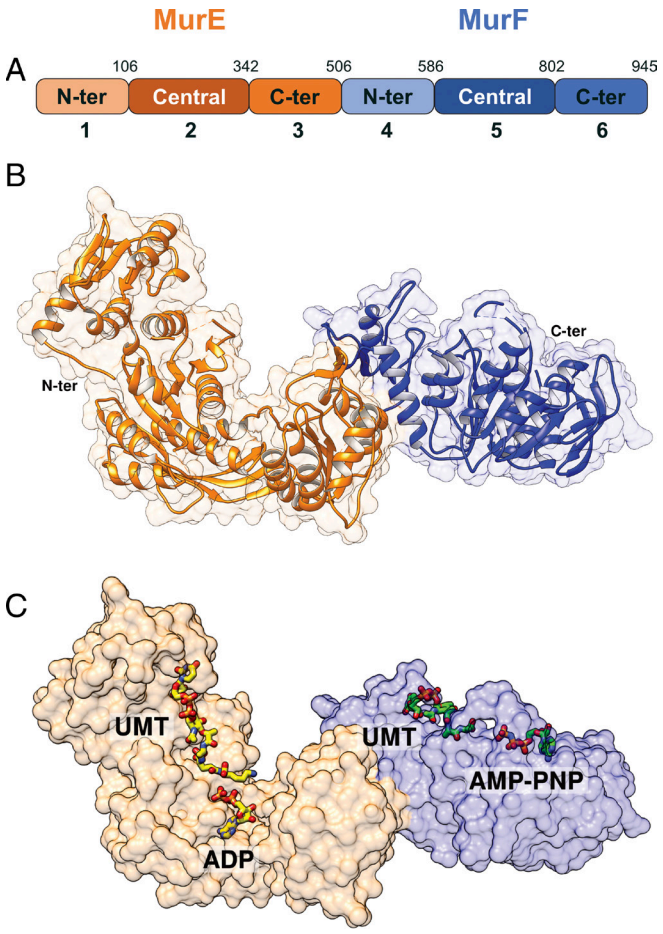

Fig. 4. MurE and MurF from *B. pertussis* are juxtaposed head-to-tail in the MurE–MurF chimera. (*A*) Schematics of the domain organization of MurE–MurF. The numbers indicate the last residue of each domain. (*B*) Ribbon representation of the MurE–MurF structure. MurE (residues 1 to 506) and MurF (residues 507 to 798) are shown in orange and blue, respectively. (*C*) Surface rendition of MurE–MurF, where the crystal structures of MurE from *S. aureus* [PDB 4CI2; (47)] and MurF from *P. aeruginosa* (PDB 4CVM) were superimposed to allow positioning of the UDPMurNAc-tripeptide substrate (UMT) and cofactors. RMSD values correspond to 1.105 Å and 1.048 Å, respectively.

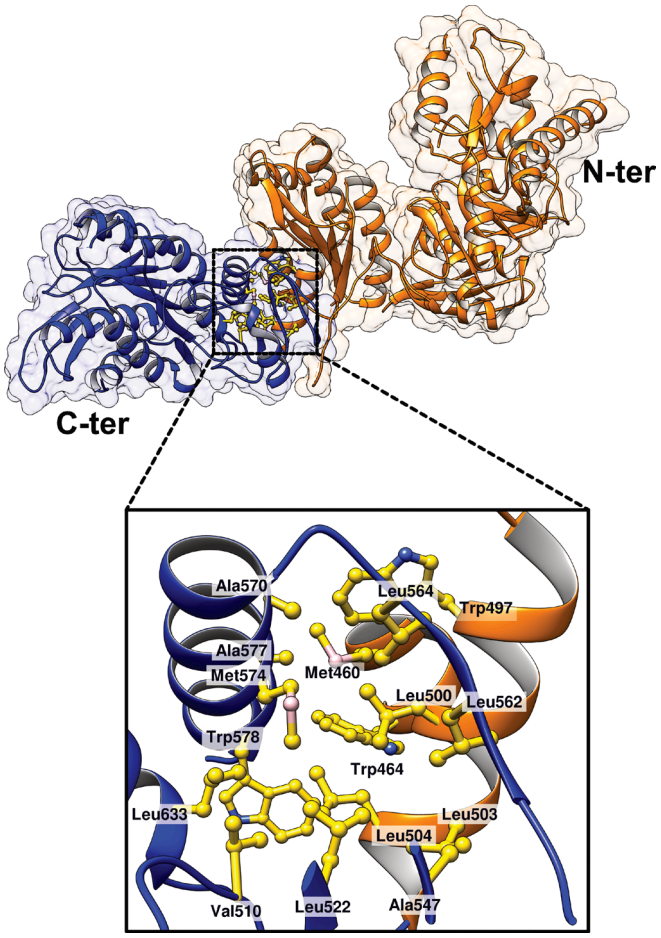

Fig. 5. The MurE–MurF interaction region is formed by a highly hydrophobic core. Side chains of residues constituting the nonpolar interaction between MurE and MurF are shown as sticks with carbon atoms in yellow, sulfur in pink, and nitrogen in blue. The MurE backbone is shown in orange, and MurF in blue.

formation of a heteromeric complex, with MurE–MurF as the central player.

In order to test whether cofactor binding could play a role in Mur ligase recognition patterns, we performed FPA experiments with MurE–$MurF_{FL}$, MurC, and MurD in the presence of ATP and its nonhydrolyzable analog AMP-PNP (Fig. 7 and *SI Appendix*, Fig. S10). Affinities in the presence of ligands were comparable to those in their absence, indicating that cofactor recognition does not play a role in complex formation. The FPA of isolated MurC and MurD in the presence of ATP and/or AMP-PNP did not yield a binding curve that allowed for K_D calculation, indicating that the presence of cofactors does not influence the recognition between MurC and MurD.

Discussion

The assembly of heteromeric protein complexes has been reported to often be facilitated by the organization of subunit-encoding genes either into operons or into clusters that largely maintain the order of required gene expression. This enables ordered translation and optimized complex assembly, which can be of significant importance in a wide range of biological processes (53). Lipid II biosynthesis is an example of a process that involves a number of highly regulated events that are involved in both cell division and cell wall elongation, and that benefits from such a gene organization scheme. PG biosynthesis has a very high turnover rate that could be favored by the formation of a multi-protein complex that could channel pathway intermediates from one protein to the next (35).

Within the *dcw* cluster of several species of proteobacteria, as well as in some archaea, certain cell wall biosynthesis proteins, such as MurE and MurF, are encoded as a single polypeptide. Since MurE and MurF catalyze two subsequent steps in PG biosynthesis, this could reflect the existence of a catalytic advantage for the cell, given that it could potentially shuttle the UM-tripeptide intermediate between the two active sites in the chimeric protein without the need for releasing the MurE catalyzed product into the cytoplasm prior to its recognition by MurF. Alternatively, after the MurE-catalyzed reaction, its product could be released and remain in the vicinity of the enzyme. This would essentially increase the local concentration of the intermediate, which could facilitate its recognition in the MurF active site. It is of note that within the MurE–MurF chimera, MurE and MurF are each independently functional, and the chimera itself is able to interact with the monomeric and oligomeric forms of MurG with a K_D of 0.6 to 1.0 μM (30), a value that is similar to those found here for MurE–MurF's interaction with MurC and MurD. These data indicate that the MurE–MurF chimera is an important actor within a potential Mur ligase complex in the cell, despite the fact that protein–protein interactions could be transient.

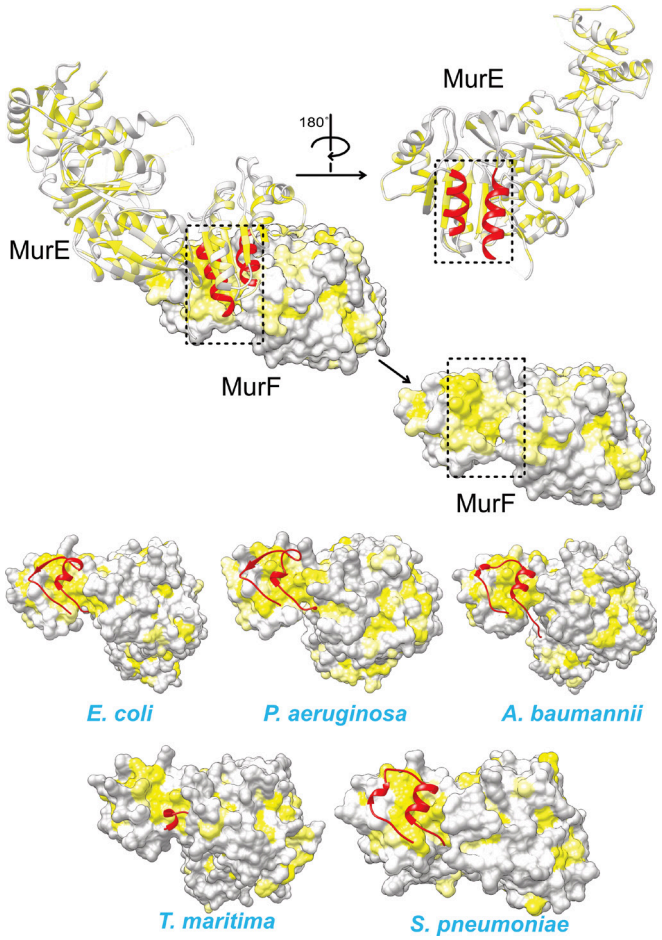

Fig. 6. MurF ligases from different species all display a cap covering a highly hydrophobic N-terminal surface. The N-terminal "caps," shown here in red, cover a hydrophobic region (yellow) on the surface of MurF. In the case of the *B. pertussis* MurE–MurF chimera, the cap is absent. Instead, this role is performed by the C-terminal region of MurE which is highlighted in red. The MurF structures used here were: *E. coli* [PDB 1GG4 (20)], *P. aeruginosa* (PDB 4CVK), *S. pneumoniae* [PDB 3ZM6 (52)], *T. maritima* [PDB 3ZL8 (29)], and *A. baumannii* [PDB 4QDI (46)].

Of the two types of MurE–MurF chimeras identified in bacterial genomes (with and without linkers), we believe that the one described in this work is a subtype of the linker-less form. Sequence analyses indicate that MurE–MurF chimeras that do not carry linkers present the sequence corresponding to the C terminus of MurE juxtaposed to the one corresponding to the N terminus of MurF (Fig. 3). Thanks to the observations made with the crystal structure, we were able to verify that the N terminus of MurF is actually missing the classic "cap" region, and a large hydrophobic patch is instead protected by MurE. This generates an intimate connection that stabilizes the chimera (i.e., we were unable to purify stable forms of constructs where intermediary domains were removed or modified). It is conceivable that many more Mur chimeras could present key interaction regions that are stabilized in this fashion.

Notably, chimeras have also been observed between MurB and MurC, MurG and MurC, MurC and Ddl, MurD and FtsW, and MraY and MurG (Figs. 1*B* and 2 and *SI Appendix*, Fig. S1). Interestingly, some of these fused proteins are formed by enzymes that do not catalyze sequential steps in the PG pathway (such as MurG/MurC, MurC/Ddl, and MurD/FtsW), and thus the idea of substrate passage between active sites to promote sequential reactions does not hold. However, chimeras could be beneficial for protein stability, as shown for the MurC–Ddl chimera of *Chlamydia trachomatis* (54). In addition, the expression of certain proteins as chimeras could play a regulatory role in the PG biosynthetic process. Ribosome profiling data from *E. coli* (where MurE and MurF are expressed as separate proteins) indicate that MurC, MurD, MurE, MurF (which are cytoplasmic), and MraY (the first membrane protein in the pathway) are expressed in the cell at similar levels. MurG however, is expressed at half their level, while FtsW is expressed at levels that are 20 to 25% those of the Mur proteins (55). It is thus tempting to propose that all reactions that lead to the biosynthesis of Lipid I, including its attachment to the C55-PP membrane component by MraY, must be regulated at the protein expression level in order to guarantee the consecutive nature of the reaction flow. This could be particularly important for Actinobacteria, of which many species carry *murG–murC* chimeras and are essentially monoderms, surrounded by a thick PG layer (25). The co-expression of enzymes that catalyze reactions at the beginning and end of the cytoplasmic reaction cycle, such as MurC and MurG, could be key for maintenance of an elevated level of murein production in the cell. Likewise, the order in which genes associate to form a chimera has been shown to be directly related to the structural features of the encoded proteins (56). It is of note that the presence of the *murC–ddl* chimera in numerous Chlamydiae also indicates that the coordinated expression of these genes is important for normal growth in these slow-growing, primarily intracellular bacteria (57).

The identification of Mur chimeras sheds light on the relevance of the co-translational folding and assembly of *mur* gene products in order to facilitate complex formation and active channeling of murein precursors to either division or elongation sites. Interestingly, it has been suggested that the divisome and the elongasome represent two competing sites for PG biosynthesis in the cell; the balance between the two sites through the tight regulation of Mur protein levels could be an additional, important factor regulating cell shape in bacteria (35). Expressing key proteins as chimeras could guarantee that they are always present at the same level in the cell, thus representing a handle to control the production of enzymes that participate in the early steps of PG biosynthesis. The expression of chimeras could also facilitate the production of kinetically unfavorable intermediates, create a controlled assembly sequence or avoid the formation of unnecessary complexes (35). Lastly, the expression of proteins as chimeras could also optimize complex assembly through the simplification of its architecture (56). This could be particularly advantageous for a cytoplasmic PG-biosynthesis complex that potentially assembles and disassembles rapidly in accordance to the point in the cell cycle.

The data presented here support the existence of a close relationship between Mur ligase interaction, complex assembly and genome evolution. The evolutionary constraint on gene order is stronger when the encoded proteins are optimized for assembly (56), as seen here in the case of the *dcw* cluster in gram-negative bacteria. In addition, evolutionary pressure to conserve gene order could arise from the intent to not disrupt the relative subunit stoichiometry (33); thus, gene fusions that encode proteins that do not catalyze successive reactions, as is the case for MurG–MurC, support the idea that these chimeras are important for the stabilization of interactions in the context of a Mur ligase complex. Thus, understanding Mur ligase assembly can lead not only to insights into bacterial genomic evolution but could also be relevant for the development of next-generation antibacterials targeting these essential enzymes.

Materials and Methods

In Silico Analyses. Sequences of Mur chimeras were obtained from Uniprot (www.uniprot.org/) by focusing on proteins from the Mur family with more than 600 amino acids (resulting in a total of 5,914 sequences in our initial dataset).

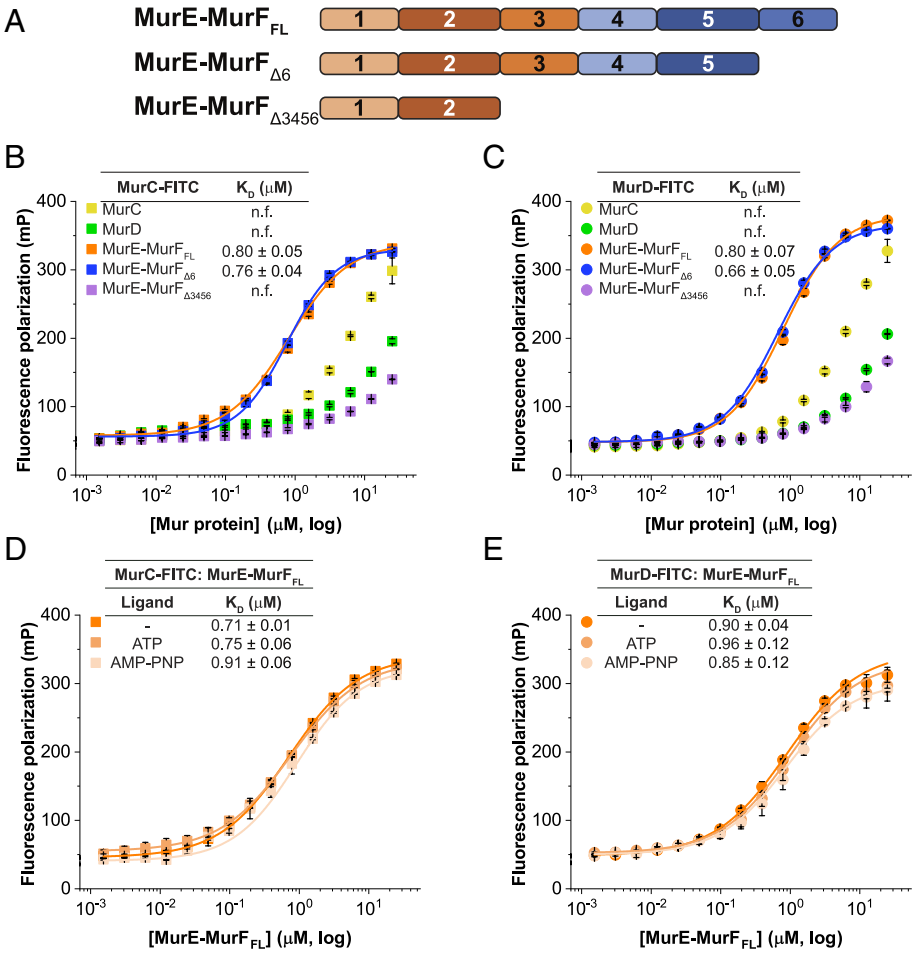

Fig. 7. MurC and MurD interact with MurE–MurF in a fluorescence polarization assay (FPA). (*A*) Schematic diagrams of MurE–MurF variants used in this study. Polarization was measured in triplicate after an incubation time of 3 h, and data were used for the calculation of K_D values. Experiments involving MurC–FITC are shown in *B*, *D* and the signal is represented with squares, while experiments involving MurD–FITC are shown in *C*, *E* and the signal is represented with dots. Note that both MurC and MurD interact with MurE–MurF$_{FL}$ and MurE–MurF$_{\Delta6}$, and that the presence of cofactors does not affect the interaction. n.f. (nonfit) indicates that a sigmoidal curve that could have allowed fitting and K_D calculation could not be measured.

The composition of Mur chimeras was confirmed by homology analysis using Interpro (www.ebi.ac.uk/interpro/). Mur chimeras from unidentified species were excluded from the dataset; a representative sequence for each identified species was selected for further analysis. Regarding the study of the distribution of major types of Mur chimeras in bacteria, SSN were generated for each type of Mur chimera using EFI-EST web [efi.igb.illinois.edu/efi-est/; (36)] and were further analyzed using Cytoscape (37).

MurE–MurF sequences were selected from the dataset and aligned with ClustalX 2.1 (58). A phylogenetic tree was constructed with iTOL v.6.5.2 (59). Taxonomy information was obtained from Uniprot, and protein lengths were based on Interpro homologies.

Regarding hydrophobic surface conservation analyses, MurE–MurF chimeras from the dataset were divided into two groups according to the presence or absence of the predicted linker region. We also analyzed the conservation of the hydrophobic patch in *Bordetella* spp, *Achromobacter* spp and other β-proteobacteria that have MurE–MurF chimeras. To analyze residue conservation in separated MurEs and MurFs, we selected MurE and MurF variants from fully annotated and identified species. Each group was aligned with the sequence of the *B. pertussis* MurE–MurF$_{FL}$ chimera using local MSA (Multiple Sequence Alignment) with Muscle v.5 (60), followed by conservation analyses with ConSurF 2016 (61). GraphPad Prism v.7 for Windows was used for the generation of graphics.

Cloning. A DNA fragment containing the *murEmurF-mraY-murD-ftsW-murG-murC* operon from the *Bordetella pertussis* (strain 18323 ATCC 9797) was amplified by PCR and inserted by In-Fusion® into two modified versions of the pBAD vector to yield constructs that could express all proteins with MurC carrying either a 10-His or a Strep-TagII at its C terminus (pBAD-Operon-His or pBAD-Operon-Strep). pBAD-Operon-His was employed as a template for the generation of MurE–MurF$_{\Delta6}$- and MurE–MurF$_{\Delta3456}$-expressing clones (pBAD–MurE–MurF$_{\Delta6}$ and pBAD–MurE–MurF$_{\Delta3456}$, respectively) through the removal of the nucleotides coding for the region between Met804 (or Arg343 for Δ3456) and the last residue of the 10-His tag, leaving just the stop codon from the vector.

The pBAD-Operon-His vector was also employed as a template for the generation of a MurD-expressing vector; *murD* was amplified using classical PCR strategies and the amplicon was cloned into pET30b. The final protein product carries an uncleavable N-terminal 8-His tag.

Construction of the MurE–MurF$_{FL}$-expressing pET15b vector, where the final protein product caries a thrombin-cleavable N-terminal 6-His tag, was previously described (30). Notably, constructs MurE–MurF$_{\Delta6}$ and MurE–MurF$_{\Delta3456}$ do not carry tags and were purified by affinity chromatography using their intrinsic affinity for the resin.

Protein Expression.

MurC, MurE–MurF$_{\Delta6}$ and MurE–MurF$_{\Delta3456}$. For MurC expression, *E. coli* BL21-AI cells were transformed with pBAD-Operon-Strep and grown at 37 °C in Terrific Broth supplemented with 200 mg/L ampicillin. For MurE–MurF$_{\Delta6}$ and MurE–MurF$_{\Delta3456}$, BL21-AI cells were transformed with pBAD–MurE–MurF$_{\Delta6}$ or pBAD–MurE–MurF$_{\Delta3456}$ and grown at 37 °C in Lysogeny Broth (LB) supplemented with 200 mg/L ampicillin. In all cases, protein expression was induced by adding 0.05% L-arabinose at OD_{600nm} = 0.8 AU, and cells were further grown for 16 h at 25 °C.

MurE–MurF$_{FL}$. *E. coli* RIL cells carrying pET15b–MurE–MurF$_{FL}$ were grown at 37 °C in LB supplemented with 200 mg/L ampicillin and 34 mg/L chloramphenicol. Expression was induced by the addition of 0.2 mM IPTG at OD_{600nm} =0.7 AU and cells were further grown for 16 h at 18 °C.

MurD. *E. coli* BL21(DE3) cells carrying pET30b–MurD were grown at 37 °C until cells reached OD_{600nm} = 0.6 AU in auto-induction medium supplemented with 50 mg/L kanamycin, and cells were further grown for 16 h at 20 °C.

Purification. After growth and induction, cells were harvested by centrifugation at 9,000 rcf, 30 min, 4 °C. Cells were resuspended in buffer A (25 mM HEPES pH 7.5, 10 mM $MgCl_2$, 300 mM NaCl, 5% glycerol) supplemented with SigmaFast™ protease inhibitor cocktail (Sigma-Aldrich), 200 μg/mL lysozyme (Sigma-Aldrich) and 250 units of benzonase (Sigma-Aldrich), and incubated in buffer A for 1 h at 4 °C. Cell lysis was performed either by passing suspended cells three times in a Microfluidizer LM20 (Microfluidics) at 18,000 psi, or by sonication (Sonics Vibracell vx500) for 15 min in cycles of 5 s ON/ 10 s OFF at 30 to 35% amplitude. Subsequently, the lysate was subjected to centrifugation at 30,000 rcf for 1 h at 4 °C, and the resulting soluble fraction of the total lysate was used for further purification steps.

MurE–MurF$_{FL}$ and MurE–MurF$_{Δ6}$. The soluble fraction of the total lysate was incubated with 5 mL of cobalt resin (Clontech Lab. Inc.) pre-equilibrated in buffer A. The mixture was applied onto an empty column and subsequently washed with 10 column volumes (cv) of buffer A to remove unbound proteins. The protein of interest was eluted from the resin with 3 cv of buffer B (25 mM HEPES pH 7.5, 10 mM $MgCl_2$, 300 mM NaCl, 5% glycerol, 300 mM imidazole). Eluted fractions were pooled and concentrated in a 50 kDa cutoff Vivaspin 15 concentrator (Sartorius). The concentrated sample was diluted 1:12 with buffer C (25 mM HEPES pH 7.5, 10 mM $MgCl_2$) for further purification by anion exchange chromatography (Mono Q 5/50 GL, GE Healthcare) and eluted in a gradient to 1 M NaCl. Fractions containing MurE–MurF$_{Δ6}$ were concentrated in a 50 kDa cutoff Vivaspin 2 concentrator (GE Healthcare) and used for crystallization trials at the Robolab high-throughput crystallization facility (LNBio, CNPEM). Fractions containing MurE–MurF$_{FL}$ were concentrated as mentioned above for MurE–MurF$_{Δ6}$ and stored at 4 °C until further use.

MurD. Affinity chromatography was carried out as described for MurE–MurF$_{FL}$. Fractions containing MurD were pooled and concentrated and the sample was further purified by size-exclusion chromatography (HiLoad Superdex 200 16/600, GE Healthcare) in buffer D (25 mM HEPES pH 7.5, 10 mM $MgCl_2$, 150 mM NaCl). Fractions containing purified MurD were pooled and concentrated in a 30 kDa cut-off Vivaspin 2 concentrator (GE healthcare) and stored at 4 °C until further use.

MurC. The soluble fraction of the total lysate was loaded onto a pre-equilibrated 5-mL Strep-trap column (Sigma-Aldrich). After 10 cv of washing in buffer A, the Strep-fused protein was eluted in buffer A supplemented with 2.5 mM d-desthiobiotin. MurC-containing fractions were pooled and concentrated in a 30 kDa cutoff Vivaspin 15 concentrator (Sartorius), and the sample was further purified by size-exclusion chromatography in buffer D. Fractions containing purified MurC were pooled and concentrated as described above for MurD.

MurE–MurF$_{Δ3456}$. The soluble fraction of the total lysate was loaded onto a pre-equilibrated 5-mL His-trap FF crude column (GE Healthcare). After 5 cv of washing in buffer A, the protein was eluted in a gradient of 0 to 500 mM imidazole. The fractions with the protein of interest were pooled, concentrated, and further purified by anion exchange as described for MurE–MurF$_{FL}$. Fractions containing the purified protein were pooled and concentrated in a 10 kDa cutoff Vivaspin 2 concentrator (Sartorius), centrifuged to remove precipitated protein, and stored at 4 °C until further use.

Proteolysis of MurE–MurF$_{FL}$. Limited proteolysis of MurE–MurF$_{FL}$ was carried out by incubating the sample with trypsin in a 1:500 protease:protein ratio (wt/wt) overnight at 4 °C. The resulting sample was analyzed by ESI-TOF mass spectrometry, which indicated that region beyond amino acid 803 had been trypsinized (62). A novel construct corresponding only to residues 1 to 803 was generated in vector pBAD, as described above.

FPAs.

Labelling of MurC and MurD. 100 to 200 μL of purified protein at ~5 mg/mL were incubated with fluorescein-5-isothiocyanate [FITC (Sigma-Aldrich)], in a five-fold molar excess, for 4 h at 4 °C in an amber Eppendorf. The protein–FITC complex was loaded onto a PD-10 desalting column (GE Healthcare) in buffer D to remove free FITC; protein–FITC fractions were stored at 4 °C in the dark.

Setup involving MurC or MurD with other Mur ligases. MurC–FITC or MurD–FITC were added to serial dilutions of the unlabeled Mur protein (MurC, MurD, MurE–MurF$_{FL}$, MurE–MurF$_{Δ6}$, MurE–MurF$_{Δ3456}$, all at 1.5 nM to 25 μM) in buffer E (25 mM HEPES pH 7.5, 10 mM $MgCl_2$, 70 mM NaCl) to a final concentration of 160 nM of MurC or MurD–FITC.

Setup involving MurC, MurD, and MurE–MurF$_{FL}$ in the presence of ligands. MurC or MurD–FITC were incubated with a 1.5 molar excess of ATP or AMP-PNP and the interactions were measured as described below. Unlabeled MurC or MurD were incubated with 1.5 molar excess of ATP or AMP-PNP; unlabeled MurE–MurF$_{FL}$ was incubated with a 3 molar excess of ATP or AMP-PNP.

α-synuclein (αSγn) control. αSγn, a small (~15 kDa) eukaryotic protein, was used as a negative control. Purified αSγn was labelled as mentioned above for MurC and MurD, and FPA was performed with either αSγn–FITC or αSγn as described for FPA studies with Mur ligases.

FP experiments were performed in black 384-well plates (Greiner Bio-One polystyrene, nonbinding flat bottom) in triplicate, and measured in a Clariostar (BMG Labtech). The FP-Endpoint detection mode was employed using a 485-nm excitation filter, a 565-nm long-pass filter and a 540-nm emission filter at 25 °C. Focus and gain adjustments for both channels were set as recommended by manufacturers. FP signals were measured after incubating the mixtures described above for 3 h at 4 °C.

Crystallization of MurE–MurF$_{Δ6}$. MurE–MurF$_{Δ6}$ diffracting crystals were obtained using two rounds of seeding optimization. Initial MurE–MurF$_{D6}$ crystals were grown by mixing 10 mg/mL of MurE–MurF$_{Δ6}$ with 85 mM HEPES pH 6.5, 1.3 M ammonium sulfate, 25% glycerol in a 1:1 ratio, to which seeding soup A was added. This seed stock was made by crushing crystals of *S. pneumoniae* MurD (grown in 100 mM Bis-Tris pH 5.5, 200 mM $MgCl_2$, 19% PEG 3350 in the presence of 1 mM AMP-PNP) and then mixing to 1:25 with equal parts of seed crystallization solution and protein sample buffer. These initial crystals appeared after 20 to 30 d and had poor/no diffraction. Hence, they were then made into a new seed stock–Seeding soup B (generated by crushing poorly diffracting MurE–MurF$_{Δ6}$ crystals and diluting them to 1:100 with crystallization solution). This was used to seed a mixture of MurE–MurF$_{Δ6}$ (at 10 mg/mL with 1 mM added ADP) and reservoir solution (1.3 M ammonium sulfate, 20% glycerol, 5% PEG3350). For microseeding purposes, the drop volume ratio used consisted of 5 parts protein (1.0 μL): four parts reservoir solution (0.8 μL):1 seeding soup (0.2 μL). All crystals were grown by using the hanging-drop vapor diffusion method at 20 °C. Single crystals were mounted in cryo-loops and transferred into a cryoprotective solution consisting of the reservoir solution and to 30% glycerol, 1 mM UMAG and 1 mM ATP were added. Crystals were flash cooled in liquid nitrogen.

Data Collection, Processing, and Structure Solution and Refinement. X-ray diffraction data were collected at the MANACÁ (MAcromolecular Micro and NAno CrystAllography) beamline/LNLS-Sirius in Campinas, Brazil, operating at 12.688 keV. Data were indexed and integrated with XDS (63). Due to diffraction anisotropy in the high-resolution shells, the dataset was anisotropy-corrected using STARANISO (Global Phasing Ltd.).

The anisotropic-corrected amplitudes were used for molecular replacement with Phaser (50). Several automatic molecular replacement programs, including MrBump (64), Balbes (65) and MoRDa (66) were initially tried but did not produce satisfactory results. The top-scoring PDBs from these programs, both truncated and nontruncated, were also selected and tested with Phaser and/or Molrep, but these methods failed to yield acceptable outcomes for refinement. Hence, a model of *B. pertussis* MurE–MurF generated by AlphaFold2 (49) was tested. The search model was split into three fragments (residues 1 to 338, 339 to 565, and 566 to 803) and a three-component search yielded the strongest MR solution. The model was then improved by iterative manual building into $2F_o–F_c$ and $F_o–F_c$ electron density maps using Coot (67). Refinement was carried out using Lorestr (68). Model quality was checked using MolProbity (69) and the wwPDB validation tool (https://validate-rcsb-2.wwpdb.org/).

The structure was deposited in the Protein Data Bank under code 8F5D. All molecular figures were prepared using Chimera 1.15 and data collection and refinement statistics are summarized in *SI Appendix*, Table S1.

Data, Materials, and Software Availability. Data (PDB coordinates) have been deposited in Protein Data Bank (8F5D) (70).

ACKNOWLEDGMENTS. We acknowledge support to A.D. from the Laboratoire International Associé BACWALL (CNRS), and grants from the São Paulo Research Foundation (FAPESP) 2011/52067-6 and 2017/12436-9. K.T.S. was supported by fellowships 2018/16346-7 and 2020/01286-9 from FAPESP, the CNPq, and CAPES. This work made use of the MANACÁ beamline of the Brazilian Synchrotron

Light Laboratory (LNLS-Sirius), the Laboratory for Bioassays (LBE) and the ROBOLAB automatic crystallization facility of the LNBio. Both LNLS and LNBio are operated by the Center for Research in Energy and Materials (CNPEM) for the Ministry for Science, Technology and Innovation (MCTI, Brazil). This work also used the platforms of the Grenoble Instruct-ERIC centre (ISBG; UAR 3518 CNRS-CEA-UGA-EMBL) within the Grenoble Partnership for Structural Biology (PSB), supported by FRISBI (ANR-10-INBS-0005-02) and GRAL, financed within the University Grenoble Alpes graduate school (Ecoles Universitaires de Recherche) CBH-EUR-GS (ANR-17-EURE-0003). The IBS acknowledges integration into the Interdisciplinary Research Institute of Grenoble (CEA). The authors wish to thank Dr. Federica Laddomada and Dr. Luca Signor (IBS mass spectrometry platform) for proteolysis experiments, Camila Canateli (CNPEM/LNBio) for the gift of purified α-Syn, and Prof. Stanislav Gobec and Dr. Martina Hrast (Univ. Ljubljana) for the gift of UM and UMA.

Author affiliations: [a]Brazilian Biosciences National Laboratory, Brazilian Center for Research in Energy and Materials, Campinas, São Paulo 13084-971, Brazil; [b]Departamento de Genética, Evolução, Microbiologia e Imunologia, Instituto de Biologia, Universidade Estadual de Campinas, CEP Campinas, São Paulo 13083-862, Brazil; and [c]Univ. Grenoble Alpes, CNRS, Commissariat à l'Energie Atomique et aux Energies Alternatives, Institut de Biologie Structurale, Bacterial Pathogenesis Group, Grenoble F-38044, France

1. P.-J. Matteï, D. Neves, A. Dessen, Bridging cell wall biosynthesis and bacterial morphogenesis. *Curr. Opin. Struct. Biol.* **20**, 749–766 (2010).
2. P.D.A. Rohs, T. Bernhardt, Growth and division of the peptidoglycan matrix. *Annu. Rev. Microbiol.* **75**, 315–36 (2021).
3. I. Nikolaidis, S. Favini-Stabile, A. Dessen, Resistance to antibiotics targeted to the bacterial cell wall. *Protein Sci.* **23**, 243–259 (2014).
4. P. Macheboeuf, C. Contreras-Martel, V. Job, O. Dideberg, A. Dessen, Penicillin Binding Proteins: Key players in bacterial cell cycle and drug resistance processes. *FEMS Microbiol. Rev.* **30**, 673–691 (2006).
5. N. Typas, M. Banzhaf, C. A. Gross, W. Vollmer, From the regulation of peptidoglycan synthesis to bacterial growth and morphology. *Nat. Rev. Microbiol.* **10**, 123–136 (2012).
6. W. Vollmer, D. Blanot, M. A. de Pedro, Peptidoglycan structure and architecture. *FEMS Microbiol. Rev.* **32**, 149–167 (2008).
7. A. Bouhss, A. E. Trunkfield, T. D. H. Bugg, D. Mengin-Lecreulx, The biosynthesis of peptidoglycan lipid-linked intermediates. *FEMS Microbiol. Rev.* **32**, 208–233 (2008).
8. I. Kouidmi, R. C. Levesque, C. Paradis-Bleau, The biology of Mur ligases as an antibacterial target. *Mol. Microbiol.* **94**, 242–253 (2014).
9. C. A. Smith, Structure, function and dynamics in the *mur* family of bacterial cell wall ligases. *J. Mol. Biol.* **362**, 640–655 (2006).
10. F. Laddomada, M. M. Miyachiro, A. Dessen, Structural insights into protein-protein interactions involved in bacterial cell wall biogenesis. *Antibiotics* **5**, 14 (2016).
11. M. Sjodt *et al.*, Structural coordination of polymerization and cross-linking by a SEDS-bPBP peptidoglycan synthase complex. *Nat. Microbiol.* **5**, 813–820 (2020).
12. A. J. Meeske *et al.*, SEDS proteins are a widespread family of bacterial cell wall polymerases. *Nature* **537**, 634–638 (2016).
13. C. Contreras-Martel *et al.*, Molecular architecture of the PBP2-MreC core bacterial cell wall synthesis complex. *Nat. Commun.* **8**, 776 (2017).
14. A. Typas *et al.*, Regulation of peptidoglycan biosynthesis by outer membrane proteins. *Cell* **143**, 1097–1109 (2010).
15. A. J. F. Egan, J. Errington, W. Vollmer, Regulation of peptidoglycan synthesis and remodelling. *Nat. Rev. Microbiol.* **18**, 446–460 (2020).
16. A. Martins *et al.*, Self-association of MreC as a regulatory signal in bacterial cell wall elongation. *Nat. Commun.* **12**, 2987 (2021).
17. P. D. A. Rohs *et al.*, A central role for PBP2 in the activation of peptidoglycan polymerization by the bacterial cell elongation machinery. *PLoS Genet.* **14**, e1007726 (2018).
18. T. Deva, E. N. Baker, C. J. Squire, C. A. Smith, Structure of *Escherichia coli* UDP-*N*-acetylmuramoyl:L-alanine ligase (MurC). *Acta Crystallogr. D Biol. Crystallogr.* **62**, 1466–1474 (2006).
19. J. A. Bertrand *et al.*, "Open" structures of MurD: Domain movements and structural similarities with folylpolyglutamate synthetase. *J. Mol. Biol.* **301**, 1257–1266 (2000).
20. Y. Yan *et al.*, Crystal structure of *Escherichia coli* UDPMurNAc-tripeptide d-alanyl-d-alanine-adding enzyme (MurF) at 2.3 Å resolution. *J. Mol. Biol.* **304**, 435–445 (2000).
21. B. C. Chung *et al.*, Crystal structure of MraY, an essential membrane enzyme for bacterial cell wall synthesis. *Science* **341**, 1012–1016 (2013).
22. S. Ha, D. Walker, Y. Shi, S. Walker, The 1.9 Å crystal structure of *Escherichia coli* MurG, a membrane-associated glycosyltransferase involved in peptidoglycan biosynthesis. *Protein Sci.* **9**, 1045–1052 (2000).
23. E. Tuomanen, J. Schwartz, S. Sande, K. Light, D. Gage, Unusual composition of peptidoglycan in *Bordetella pertussis*. *J. Biol. Chem.* **264**, 11093–11098 (1989).
24. Y. A. Nikolaichik, W. D. Donachie, Conservation of gene order amongst cell wall and cell division genes in Eubacteria, and ribosomal genes in Eubacteria and Eukaryotic organelles. *Genetica* **108**, 1–7 (2000).
25. R. R. Léonard *et al.*, Was the last bacterial common ancestor a monoderm after all? *Genes* **13**, 376 (2022).
26. G. Real, A. O. Henriques, Localization of the Bacillust subtilis *murB* gene within the dcw cluster is important for growth and sporulation. *J. Bacteriol.* **188**, 1721–1732 (2006).
27. M. Pilhofer *et al.*, Characterization and evolution of cell division and cell wall synthesis genes in the bacterial phyla *Verrucomicrobia*, *Lentisphaerae*, *Chlamydiae*, and *Planctomycetes* and phylogenetic comparison with rRNA genes. *J. Bacteriol.* **190**, 3192–3202 (2008).
28. J. Tamames, Evolution of gene order conservation in prokaryotes. *Genome Biol.* **2**, research0020.1 (2001).
29. S. Favini-Stabile, C. Contreas-Martel, N. Thielens, A. Dessen, MreB and MurG as scaffolds for the cytoplasmic steps of peptidoglycan biosynthesis. *Environ. Microbiol.* **15**, 3218 (2013).
30. F. Laddomada *et al.*, The MurG glycosyltransferase provides an oligomeric scaffold for the cytoplasmic steps of peptidoglycan biosynthesis in *Bordetella pertussis*. *Sci. Rep.* **9**, 4656 (2019).
31. C. L. White, A. Kitich, J. W. Gober, Positioning cell wall synthetic complexes by the bacterial morphogenetic proteins MreB and MreD. *Mol. Microbiol.* **76**, 616–633 (2010).
32. M. M. Miyachiro *et al.*, Complex formation between Mur enzymes from *Streptococcus pneumoniae*. *Biochemistry* **58**, 3314–3324 (2019).
33. J. N. Wells, T. Bergendahl, J. A. Marsh, Operon gene order is optimized for ordered protein complex assembly. *Cell Rep.* **14**, 679–685 (2016).
34. L. L. Silver, Challenges of antibacterial discovery. *Clin. Microbiol. Rev.* **24**, 71–109 (2011).
35. J. Mingorance, J. Tamames, M. Vicente, Genomic channeling in bacterial cell division. *J. Mol. Recognit.* **17**, 481–487 (2004).
36. R. Zallot, N. Oberg, J. A. Gerlt, The EFI web resource for genomic enzymology tools: Leveraging protein, genome, and metagenome databases to discover novel enzymes and metabolic pathways. *Biochemistry* **58**, 4169–4182 (2019).
37. P. Shannon *et al.*, Cytoscape: A software environment for integrated models of biomolecular interaction networks. *Genome Res.* **13**, 2498–2504 (2003).
38. I. Vaz-Moreira *et al.*, *Candidimonas nitroreducens* gen. nov., sp. nov. and *Candidimonas humi* sp. nov., isolated from sewage sludge compost. *Int. J. Syst. Evol. Microbiol.* **61**, 2238–2246 (2011).
39. B. Cao *et al.*, Complete genome sequence of *Pusillimonas* sp. T7–7, a cold-tolerant diesel oil-degrading bacterium isolated from the Bohai Sea in China. *J. Bacteriol.* **193**, 4021–4022 (2011).
40. Q.-M. Liu, L. N. Ten, W.-T. Im, S.-T. Lee, *Castellaniella caeni* sp. nov., a denitrifying bacterium isolated from sludge of a leachate treatment plant. *Int. J. Syst. Evol. Microbiol.* **58**, 2141–2146 (2008).
41. B. Isler, T. J. Kidd, A. G. Stewart, P. Harris, D. L. Paterson, *Achromobacter* infections and treatment options. *Antimicrob. Agents Chemother.* **64**, 733–736 (2020).
42. L. Saiman *et al.*, Identification and antimicrobial susceptibility of *Alcaligenes xylosoxidans* isolated from patients with cystic fibrosis. *J. Clin. Microbiol.* **39**, 3942–3945 (2001).
43. L. Ma *et al.*, Natural history and ecology of interactions between *Bordetella* species and amoeba. *Front. Cell. Infect. Microbiol.* **12**, 798317 (2022).
44. H. Finger, C. H. W. Von Koenig, "Bordetella" in *Medical Microbiology*, S. Baron, Ed. (University of Texas Medical Branch at Galveston, ed. 4, 1996).
45. M. Madhaiyan *et al.*, *Pleomorphomonas diazotrophica* sp. nov., an endophytic N-fixing bacterium isolated from root tissue of *Jatropha curcas* L. *Int. J. Syst. Evol. Microbiol.* **63**, 2477–2483 (2012).
46. S. S. Cha, Y. J. An, C. S. Jeong, J. H. Yu, K. M. Chung, ATP-binding mode including a carbamoylated lysine and two Mg(2+) ions, and substrate-binding mode in *Acinetobacter baumannii* MurF *Biochem. Biophys. Res. Commun.* **450**, 1045–1050 (2014).
47. K. M. Ruane *et al.*, Specificity determinants for lysine incorporation in *Staphylococcus aureus* peptidoglycan as revealed by the structure of a MurE enzyme ternary complex. *J. Biol. Chem.* **288**, 33439–33448 (2013).
48. K. H. Jung *et al.*, Wide-open conformation of UDP-MurNc-tripeptide ligase revealed by the substrate-free structure of MurE from *Acinetobacter baumannii*. *FEBS Lett.* **595**, 275–283 (2021).
49. M. Mirdita *et al.*, ColabFold: Making protein folding accessible to all. *Nat. Methods* **19**, 679–682 (2022).
50. A. J. McCoy *et al.*, Phaser crystallographic software. *J. Appl. Cryst.* **40**, 658–674 (2007).
51. R. Šink *et al.*, Crystallographic study of peptidoglycan biosynthesis enzyme MurD: Domain movement revisited. *PLoS One* **11**, e0152075 (2016).
52. M. Hrast *et al.*, Structure-activity relationships of new cyanothiophene inhibitors of the essential peptidoglycan biosynthesis enzyme MurF. *Eur. J. Med. Chem.* **66**, 32–45 (2013).
53. E. Natan, J. N. Wells, S. A. Teichmann, J. A. Marsh, Regulation, evolution and consequences of cotranslational protein complex assembly. *Curr. Opin. Struct. Biol.* **42**, 90–97 (2017).
54. A. J. McCoy, A. T. Maurelli, Characterization of *Chlamydia* MurC-Ddl, a fusion protein exhibiting D-alanyl-D-alanine ligase activity involved in peptidoglycan synthesis and D-cycloserine sensitivity. *Mol. Microbiol.* **57**, 41–52 (2005).
55. G.-W. Li, D. Burkhardt, C. Gross, J. S. Weissman, Quantifying absolute protein synthesis rates reveals principles underlying allocation of cellular resources. *Cell* **157**, 624–635 (2014).
56. J. A. Marsh *et al.*, Protein complexes are under evolutionary selection to assemble via ordered pathways. *Cell* **153**, 461–470 (2013).
57. L. Hesse *et al.*, Functional and biochemical analysis of *Chlamydia trachomatis* MurC, an enzyme displaying UDP-N-acetylmuramate:amino acid ligase activity. *J. Bacteriol.* **185**, 6507–6512 (2003).
58. M. A. Larkin *et al.*, Clustal W and Clustal X version 2.0. *Bioinformatics* **23**, 2947–2948 (2007).
59. I. Letunic, P. Bork, Interactive tree of life (iTOL) v5: An online tool for phylogenetic tree display and annotation. *Nucleic Acids Res.* **49**, W293–W296 (2021).
60. R. C. Edgar, MUSCLE: Multiple sequence alignment with high accuracy and high throughput. *Nucleic Acids Res.* **32**, 1792–1797 (2004).
61. H. Ashkenazy *et al.*, ConSurf 2016: An improved methodology to estimate and visualize evolutionary conservation in macromolecules. *Nucleic Acids Res.* **44**, W344–W350 (2016).
62. F. Laddomada, "Structure et assemblage de complexes des enzymes Mur, essentielles pour la synthèse de la paroi bactérienne", Université Grenoble Alpes, Grenoble, France (2016).
63. W. Kabsch, XDS. *Acta Crystallogr. D Biol. Crystallogr.* **66**, 125–132 (2010).
64. R. M. Keegan, M. D. Winn, MrBUMP: An automated pipeline for molecular replacement. *Acta Crystallogr. D Biol. Crystallogr.* **64**, 119–124 (2008).
65. F. Long, A. A. Vagin, P. Young, G. N. Murshudov, BALBES: A molecular replacement pipeline. *Acta Crystallogr. D Biol. Crystallogr.* **64**, 125–132 (2008).
66. A. Vagin, A. Lebedev, MoRDa, an automatic molecular replacement pipeline. *Acta Crystallogr. Sect. A* **A71**, 44 (2015).
67. P. Emsley, B. Lohkamp, W. G. Scott, K. Cowtan, Features and development of Coot. *Acta Crystallogr. D Biol. Crystallogr.* **66**, 486–501 (2010).
68. R. A. Nicholls, O. Kovalevskiy, G. N. Murshudov, Low resolution refinement of atomic models against crystallographic data. *Methods Mol. Biol.* **1607**, 565–593 (2017).
69. V. B. Chen *et al.*, MolProbity: All-atom structure validation for macromolecular crystallography. *Acta Crystallogr. D Biol. Crystallogr.* **66**, 12–21 (2010).
70. K. T. Shirakawa *et al.*, *Architecture* of the MurE-MurF ligase bacterial *cell* wall biosynthesis complex. *RCSB Protein* Data Bank. https://www.rcsb.org/structure/8F5D. Deposited 14 November 2022.